Original Article

Mitochondria-specific peptide amphiphiles induce mitochondrial dysfunction and peripheral T-cell lymphomas (PTCL) damage

Qi Sun[1#], Ailing Gui[1#], Aihua Zou[2], Yichen Yan[1], Shi Qiu[1], Shun Zhu[1], Wen Liu[1], Ji Zuo[1], Qunling Zhang[3,4], Ling Yang[1]

[1]Department of Cellular and Genetic Medicine, School of Basic Medical Sciences, Fudan University, Shanghai, China; [2]College of Chemistry and Materials Science, Shanghai Normal University, Shanghai, China; [3]Department of Lymphoma, Fudan University Shanghai Cancer Center, Shanghai, China; [4]Department of Oncology, Shanghai Medical College, Fudan University, Shanghai, China

Contributions: (I) Conception and design: L Yang, Q Zhang, A Zou; (II) Administrative support: L Yang, Q Zhang, J Zuo; (III) Provision of study materials or patients: L Yang, Q Zhang, W Liu; (IV) Collection and assembly of data: Q Sun, A Gui; (V) Data analysis and interpretation: Q Sun, A Gui, Y Yan, S Qiu, S Zhu; (VI) Manuscript writing: All authors; (VII) Final approval of manuscript: All authors.

[#]These authors contributed equally to this work.

Correspondence to: Ling Yang. Department of Cellular and Genetic Medicine, School of Basic Medical Sciences, Fudan University, Shanghai, China. Email: yangling@fudan.edu.cn; Qunling Zhang. Department of Lymphoma, Fudan University Shanghai Cancer Center, Shanghai, China; Department of Oncology, Shanghai Medical College, Fudan University, Shanghai, China. Email: zhangqunling@fudan.edu.cn.

Background: Peripheral T-cell lymphomas (PTCL) are aggressive lymphomas with poor prognosis, and therefore, there is a pressing need to explore new targets or compounds. Mitochondria may serve as a potential therapeutic target for PTCL. A designed positively-charged segment (pKV) is anchored to the specific 15 amino acid sequence (MIASHLLAYFFTELN) to yield a cell-penetrating peptide (pHK-pKV) and a lipid chain (Pal) is conjugated to the N-terminus of pHK-pKV (Pal-pHK-pKV) are bioactive amphiphilic peptide assemblies targeting the interaction between mitochondrial voltage dependent anion channel 1 (VDAC1) and hexokinase II (HKII).

Methods: PTCL cell line H9 was treated with Pal-pHK-pKV and pHK-pKV, respectively. Cell proliferation in each group was measured by detecting cell viability and the corresponding marker Ki-67. Apoptosis was detected by immunofluorescence, flow cytometry and western blot. We also measured mitochondrial membrane potential, adenosine triphosphate (ATP) production, the cytochrome c distribution and the expression levels of B cell lymphoma 2 (*BCL-2*) and BCL-2 associated X protein (*BAX*). Western blot was used to detect the activation of the extracellular regulated protein kinases (ERK) signaling pathway.

Results: Pal-pHK-pKV and pHK-pKV with 20 μM blocked the interaction between VDAC1 and HKII, and detached HKII from mitochondria, which depolarized the mitochondrial membrane potential, induced mitochondria dysfunction, and decreased ATP production. The decreased ATP subsequently inhibited the activation of the ERK/BCL-2 pathway and increased the BAX/BCL-2 ratio. Cytochrome c was then released from the mitochondria and induced capase-3 activation and subsequently apoptosis. Additionally, decreased ATP induced the expression of *FAS* and then apoptosis.

Conclusions: Mitochondria specific peptide amphiphiles induce mitochondrial dysfunction and provide a new approach for the treatment of PTCL.

Keywords: Amphiphilic peptides; peripheral T-cell lymphoma (PTCL); mitochondrial dysfunction; apoptosis

Submitted Mar 29, 2022. Accepted for publication May 17, 2022.
doi: 10.21037/atm-22-2233
View this article at: https://dx.doi.org/10.21037/atm-22-2233

Introduction

Peripheral T-cell lymphoma (PTCL) is a malignant lymphoproliferative disease accounting for 5–15% of all non-Hodgkin's lymphomas (NHL) (1). PTCL is derived from mature T lymphocytes with several distinct entities, among which PTCL-not otherwise specified (PTCL-NOS), angioimmunoblastic T-cell lymphoma (AITL), anaplastic lymphoma kinase (ALK)-positive anaplastic large cell lymphoma (ALCL), and ALK-negative ALCL are the most common subtypes. PTCL is an aggressive lymphoma with a poor prognosis. Although standard treatment with anthracycline-based chemotherapy, such as cyclophosphamide, doxorubicin, vincristine, prednisone with or without etoposide (CHOPE or CHOP), combined with autologous stem cell transplantation (ASCT) consolidation in high-risk patients, the outcomes remain bleak for PTCL-NOS and AITL, with 5-year overall survival (OS) rates of only 32–35% (2-4). Furthermore, traditional chemotherapy regimens have poor responsiveness and short durable remission. Therefore, there is a pressing need to explore new targets or drugs for the treatment of PTCL.

The oncogenesis of PTCL is complex; the dysregulation of T cell receptor (TCR) downstream signaling pathways is one major cause, including nuclear factor kappa-B (NF-κB), phosphatidylinositol-3-kinase (PI3K), extracellular regulated protein kinases (ERK), and janus kinase (JAK)-signal transducer and activator of transcription (STAT) signaling pathway activation (5-7). Mitochondria are essential organelles that generate most of the chemical energy for the biochemical reactions of cells through adenosine triphosphate (ATP) production. So, mitochondria are very important in normal signal transduction (8) and TCR signal activation. Moreover, TCR-mediated activation is tightly related to the cellular metabolic changes, TCR activation can promote the aerobic glycolysis and enhance the T cell function (9,10). The glycolytic metabolism may promote the translocation of hexokinase-II and inhibit cell apoptosis (11). Hence, mitochondria can serve as a PTCL therapeutic target.

The overexpression of Hexokinase II (HKII) and its interaction with mitochondrial voltage-dependent anion channel 1 (VDAC1) are critical for cancer cell proliferation via the inhibition of apoptosis (12-14). A previous study has shown that the first 10–20 amino acids in N-terminal of HKII are responsible for binding to VDAC1 (15). Thus, novel compounds, which block the binding of HKII to VDAC, can be used in cancer therapy. Liu *et al.* designed two cell-penetrating peptides, a designed positively-charged segment (pKV) is anchored to the specific 15 amino acid sequence (MIASHLLAYFFTELN) to yield a cell-penetrating peptide (pHK-pKV) and a lipid chain (Pal) is conjugated to the N-terminus of pHK-pKV (Pal-pHK-pKV), which can inhibit the growth of non-small cell lung cancer cells via apoptosis (16). pHK-pKV has a positively charged segment anchored to the HKII-VDAC1 interaction sequence, and Pal-pHK-pKV conjugates a lipid chain (Pal) with a hydrophobic palmitic acid moiety at the N-terminus, which can increase the intracellular delivery ability to the pHK-pKV. In addition, Pal-pHK-pKV conjugates have an enhanced bioactivity in terms of the degree of cellular uptake, and mitochondrial localization (16). At present, the anti-tumor activity of Pal-pHK-pKV and pHK-pKV in PTCL is unknown, and is worthy of further investigation.

In this study, we found that Pal-pHK-pKV and pHK-pKV inhibited the growth of PTCL in a dose- and time-dependent manner. The morphology and function of mitochondria were damaged, and ATP production was decreased after treatment with Pal-pHK-pKV and pHK-pKV. As a result, Pal-pHK-pKV and pHK-pKV induced apoptosis in PTCL by inhibiting the ERK pathway, enhancing the B cell lymphoma 2 associated X protein (BAX)/B cell lymphoma 2 (BCL-2) ratio, promoting the release of cytochrome c, and inducing the expression of *FAS*. We present the following article in accordance with the MDAR reporting checklist (available at https://atm.amegroups.com/article/view/10.21037/atm-22-2233/rc).

Methods

Cells and cell culture

The H9 cell, a human T-cell lymphoma cell line, was purchased from ATCC (HTB-176, ATCC, USA). The cells were cultured in roswell park memorial institute (RPMI) 1640 (MA0215, Meilunbio, China) supplemented with 10% fatal bovine serum (FBS) (10099141, Gibco, USA) containing penicillin (100 U/mL) and streptomycin (100 μg/mL) (MA0110, Meilunbio, China). The H9 cell line used in our study was mycoplasma negative detected by polymerase chain reaction (PCR) with two primer pairs, which was summarized in *Table 1*.

Cell viability assay

The cell counting kit-8 (CCK-8, MA0218, Meilunbio,

Table 1 All sequences of qPCR primers in text

Name	Forward	Reverse
FAS	TCTGGTTCTTACGTCTGTTGC	CTGTGCAGTCCCTAGCTTTCC
BCL-2	GGTGGGGTCATGTGTGTGG	CGGTTCAGGTACTCAGTCATCC
BAX	CCCGAGAGGTCTTTTTCCGAG	CCAGCCCATGATGGTTCTGAT
GAPDH	GGAGCGAGATCCCTCCAAAAT	GGCTGTTGTCATACTTCTCATGG
Mycoplasma assay 1	GGCGAATGGGTGAGTAACACG	CGGATAACGCTTGCGACCTATG
Mycoplasma assay 2	GGGAGCAAACAGGATTAGATACCCT	TGCACCATCTGTCACTCTGTTAACCTC

qPCR, quantitative real-time PCR.

China) was used to measure cell viability. A 200 µL cell suspension from different groups (1×10^5 cells/mL) was seeded into each well of a 96-well plate. After incubation for the indicated time (24, 48, 72, and 96 h), 10 µL of water-soluble tetrazolium dye (WST)-8 solution was added to each well, and the cells were cultured at 37 ℃ for another 1 h. The optical density (OD) of the cells was then measured using a microplate reader (Synergy 2, BioTek, USA) at 450 nm. We did a pilot study before the experiment. We found there was no difference between 1–10 µM, and the maximum tolerated dose is 50 µM. Therefore, we only choose representative presentations.

Quantitative real-time PCR

The RNAsimple Total RNA Kit (DP419, TIANGEN, China) was used for ribonucleic acid (RNA) extraction. Next, the messenger RNA (mRNA) was quantified, and a total of 1 µg mRNA from each sample was reversely transcribed by a 1st Strand complementary DNA (cDNA) Synthesis SuperMix (11123ES60, YEASEN, China) in 20 µL volume for 30 min at 42 ℃ and subsequently for 5 min at 85 ℃. The quantitative real-time PCR was performed using a Real-Time PCR System (Applied Biosystems, USA) in 96-well plates with a 10 µL reaction volume containing 2 µL cDNA, 50 nM forward and reverse primers, and SYBR Green Master Mix (11203ES03, YEASEN, China). Each sample was examined in triplicate. PCR reactions were performed for 40 cycles after 10 min of denaturation at 95 ℃. Each cycle consisted of 15 s of denaturation at 95 ℃, 1 min of annealing at 60 ℃, and 1 min of extension at 72 ℃. The primer pairs for human genes used in the present experiments were summarized in *Table 1*.

Immunofluorescence

For immunofluorescence staining, the cells on glass coverslips were incubated with rabbit anti-Ki-67 antibody (ab16667, Abcam, UK) at a dilution of 1:200 with rabbit anti-cleaved caspase 3 antibody (9664, Cell Signaling Technology, USA) at a dilution of 1:100. After washing three times in phosphate buffer saline (PBS), the samples were incubated with donkey anti-rabbit Alexa Fluor 594 antibody for Ki-67 (R37119, Invitrogen, USA, 1:400) detection and a donkey anti-rabbit Alexa Fluor 488 antibody (A21206, Invitrogen, USA, 1:400) for cleaved caspase 3 detection for 30 min at room temperature. Next, the nuclei were counterstained with 4,6-diamidino-2-phenylindole (DAPI) (MA0128, Meilunbio, China), and the photos were captured by a fluorescence microscope (Olympus BX53, Japan) and analyzed using Adobe Photoshop CS 6.0 software (Adobe, USA).

For mitotracker staining, T-cell lymphoma cells were stained with Mitotracker (M7512, Invitrogen, USA, 1:2,000). The slides were then mounted with anti-fading mounting medium (with DAPI) (MA0236, Meilunbio, China).

For measurement of mitochondrial membrane potential ($\Delta\psi m$), the H9 cells were planted at a density of 1×10^6/well in six-well plates, and then treated with 10 µM Pal-pHK-pKV or pHK-pKV at 37 ℃ for 30 min. The $\Delta\psi m$ was measured using a J-aggregates cyanine dye (JC)-1 kit (C2006, Beyotime, China) according to the manufacturer's instructions. The positive signals were detected by confocal microscope system (X-LIGHT V2 spinning disk confocal, 89 North; Leica DMi8 microscope, Leica). Adobe Photoshop CS 6.0 software were used to analyze the captured images.

Western blot

3×10^6 cells from each group were harvested and lysed in 200 µL radio immunoprecipitation assay (RIPA) lysis buffer containing proteinase and phosphatase inhibitor cocktails (MA0151, Meilunbio, China; MB2678, Meilunbio, China; 1:100), and the supernatants were mixed with an equal amount of 2× loading buffer and boiled for 5 min. Next, the protein samples were separated by a 10% sodium dodecyl sulfate polyacrylamide gel electrophoresis (SDS-PAGE) (AP15L945, Life-iLab, China) and transferred onto a polyvinylidene difluoride (PVDF) membrane (IPVH00010, Millipore, USA). After blocking with 5% skimmed milk for 1 h, the membranes were incubated with primary antibodies overnight at 4 ℃. After washing three times with tris buffered saline (TBS) containing 0.1% Tween-20 (T8220, Solarbio, China), the membranes were incubated with a goat anti-mouse or a goat anti-rabbit horseradish peroxidase (HRP)-conjugated immunoglobin G (IgG) antibody (AS003; AS014, ABclonal, China, 1:5,000) at room temperature for 1 h. The proteins were visualized by a Molecular Imager ChemiDoc XRS System (Bio-Rad) using a super sensitive enhanced chemiluminescence (ECL) reagent (MA0186, Meilunbio, China).

The following primary antibodies were used: anti-AKT antibody (A17909, ABclonal, China, 1:1,000), anti-phospho-AKT antibody (AP0637, ABclonal, China, 1:1,000), anti-ERK1/2 antibody (4695, Cell Signaling Technology, USA, 1:2,000), anti-phospho-ERK1/2 antibody (4370, Cell Signaling Technology, USA, 1:2,000), anti-p38 antibody (9212, Cell Signaling Technology, USA, 1:2,000), anti-phospho-p38 antibody (9215, Cell Signaling Technology, USA, 1:2,000), anti-BAX antibody (50599-2, Proteintech, USA, 1:1,000), anti-BCL-2 antibody (12789-1, Proteintech, USA, 1:1,000), anti-GAPDH (60004-1, Proteintech, USA, 1:2,000), and anti-β-actin antibody (AC004, Abclonal, China, 1:2,000).

Measurement of ATP

The H9 cells were treated with 5 µM of Pal-pHK-pKV or pHK- pKV at 37 ℃ for 48 h. Subsequently, the cells and medium were collected in tubes and centrifuged at 4 ℃, and the cell-free supernatant was used to detect ATP concentrations using an ATP Determination Kit (4695, Cell Signaling Technology, USA, 1:2,000) and a luminometer.

Fluorescence activated cell sorting (FACS) analysis

For apoptosis detection, the cells were prepared and treated with or without pHK-pKV or Pal-pHK-pKV at a concentration of 5 µM for 48 h at 37 ℃. 1×10^5 cells were collected and washed twice with PBS, and then resuspended by 100 µL binding buffer. Next, 5 µL of Annexin and propidium iodide (PI) from an apoptosis kit (MB0220, Meilunbio, China) were added to each tube and incubated in the dark for 15 min at room temperature. Apoptosis was then measured by flow cytometry (FACSCanto II, BD), and the data was analyzed by FlowJo V10 (BD).

For measurement of $\Delta\psi m$, JC-1 staining was performed as described above. The other aliquot of each sample was resuspended in PBS and analyzed by flow cytometry.

Statistical analysis

All data were analyzed using a two-tailed Student's *t*-test or one-way analysis of variance (ANOVA) using GraphPad Prism software (GraphPad, USA). $P<0.05$ was considered statistically significant. Data were presented as means ± standard deviation (SD). Each experiment was independently repeated three technical replicates.

Results

Mitochondria-specific peptide amphiphiles inhibit PTCL H9 cell proliferation

To investigate the effects of mitochondria-specific peptides on PTCL, the PTCL cell line H9 cells were treated with different concentrations of pHK-pKV and Pal-pHK-pKV for 48 h, respectively. The results (*Figure 1A*) showed that pHK-pKV and Pal-pHK-pKV significantly decreased the viability of H9 cells at concentrations of up to 20 µM. At the same time, cell viability was markedly lower in Pal-pHK-pKV-treated cells compared to pHK-pKV-treated cells at the same concentration. The viability of pHK-pKV-treated cells was about 50% at a concentration of 20 µM, but the cell viability in the Pal-pHK-pKV-treated group was only 25%. Moreover, 20 µM of pHK-pKV and Pal-pHK-pKV could also inhibit cell proliferation in a time-dependent manner (*Figure 1B*). Furthermore, Pal-pHK-pKV exhibited notably higher inhibition efficiency than pHK-pKV. Meanwhile, through immunofluorescence staining, we found that the Ki-67-positive cells were

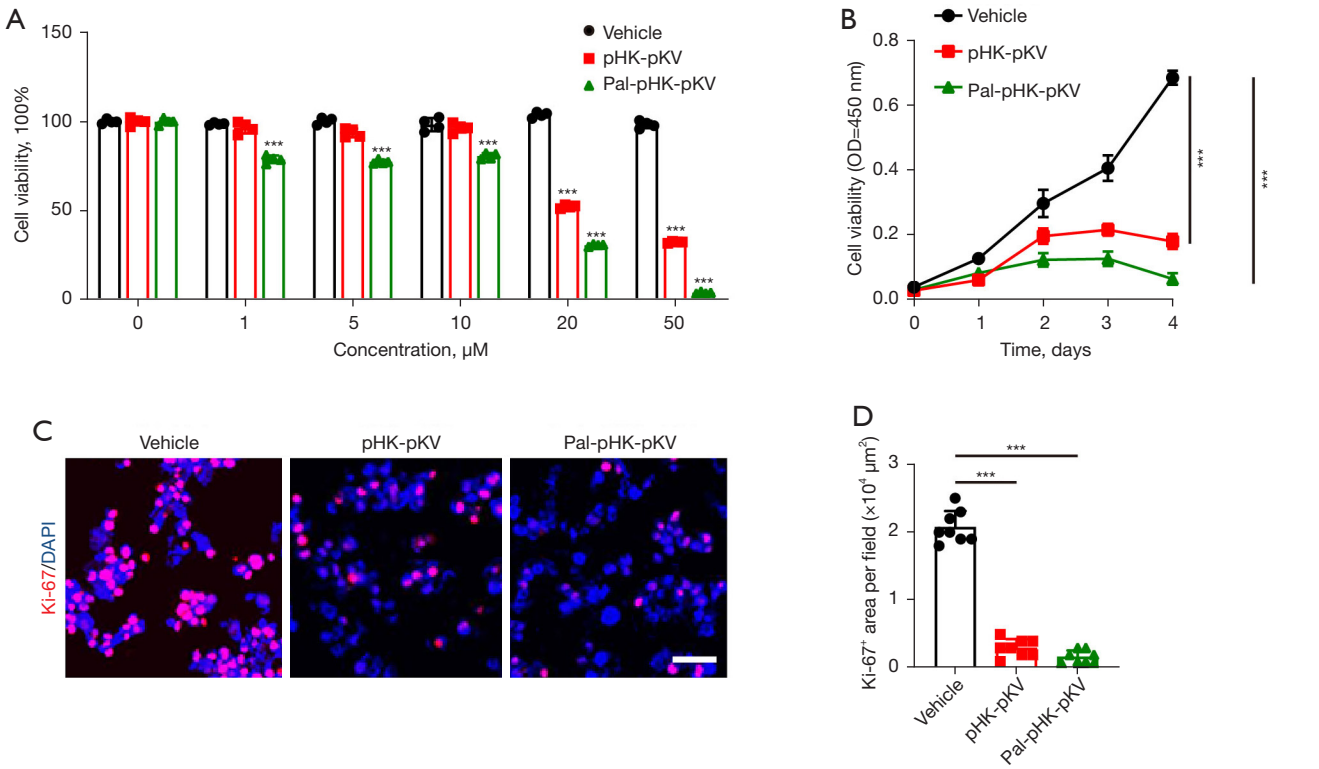

Figure 1 pHK-pKV and Pal-pHK-pKV inhibited PTCL H9 cell proliferation. (A) The viability of H9 cells treated with pHK-pKV and Pal-pHK-pKV at different concentrations (1, 5, 10, 20, 50 μM) for 48 h. (B) The growth rates of H9 cells *in vitro* with pHK-pKV and Pal-pHK-pKV treatment (n=5 samples per group). (C) Immunofluorescence staining for Ki-67 (red) and DAPI (blue) in various groups. Scale bar =50 μm. (D) Quantification of positive Ki-67 staining cells (n=8 random fields per group). ***P<0.001. Data were presented as mean ± SD. PTCL, peripheral T-cell lymphomas.

significantly decreased in the Pal-pHK-pKV and pHK-pKV groups compared to the control group (*Figure 1C*,*1D*).

Mitochondria-specific peptide amphiphiles induce PTCL H9 cell apoptosis

Compared to the control group, the cleaved caspase-3-positive cells detected by immunofluorescence staining increased in the pHK-pKV group and obviously increased in the Pal-pHK-pKV group (*Figure 2A*,*2B*). Furthermore, the number of apoptotic cells was calculated by flow cytometry analysis. The result showed that the apoptotic cell ratio in the pHK-pKV group was higher than that in the control group and even more significantly higher in the Pal-pHK-pKV group (*Figure 2C*,*2D*). Taken together, these results indicated that Pal-pHK-pKV and pHK-pKV both induced H9 cell apoptosis, and Pal-pHK-pKV induced cell apoptosis to a greater degree than pHK-pKV.

Mitochondria-specific peptide amphiphiles induce mitochondrial dysfunction

In order to explain the possible mechanism of the decreased proliferation and increased apoptosis induced by Pal-pHK-pKV and pHK-pKV, confocal microscopy was used to observe the mitochondrial distribution and morphology. Mitochondria were aggregated with Pal-pHK-pKV and pHK-pKV treatment, and were evenly distributed around the nucleus in the control group (*Figure 3A*). The pHK-pKV also altered the mitochondrial morphology, which was altered even more obviously with Pal-pHK-pKV (*Figure 3A*).

To further explore the roles of Pal-pHK-pKV and pHK-pKV on mitochondrial function, mitochondrial membrane potential (MMP) was measured through confocal microscopy and flow cytometry using JC-1. The results showed Pal-pHK-pKV significantly induced MMP dysfunction, but pHK-pKV only slightly influenced MMP

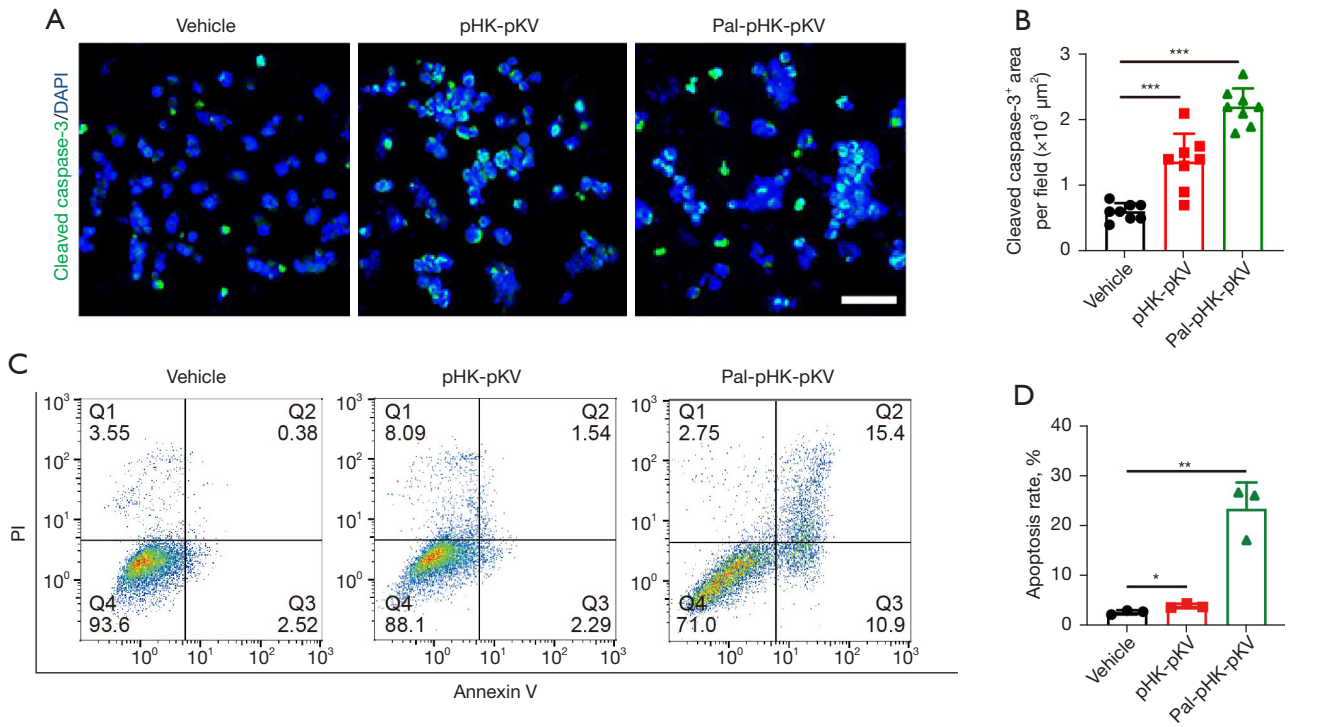

Figure 2 pHK-pKV and Pal-pHK-pKV induced PTCL H9 cell apoptosis. (A) Representative immunofluorescence staining of cleaved caspase-3 (green) and DAPI (blue) in various groups. Scale bar =50 μm. (B) Quantification of cleaved caspase-3 positive cells (n=8 random fields per group). (C) Representative FACS image of PI and Annexin V staining of vehicle, pHK-pKV-treated, and Pal-pHK-pKV-treated H9 cells. (D) Quantification of the percentages of apoptotic cells (n=3 samples per group). *P<0.05; **P<0.01; ***P<0.001. Data were presented as mean ± SD. PTCL, peripheral T-cell lymphomas; DAPI, 4,6-diamino-2-phenyl indole; FACS, fluorescence activated cell sorting; PI, propidium iodide.

(*Figure 3B,3C*). At the same time, Pal-pHK-pKV and pHK-pKV induced the decrease of ATP production compared to the control cells (*Figure 3D*).

Mitochondria-specific peptide amphiphiles induce apoptosis through ERK/BCL-2 pathway

To investigate which signalling pathway was involved in the apoptosis induced by mitochondria-specific peptides, western blot was used to detect the activation of the AKT, ERK, and P38 signal pathways. Interestingly, only phospho-ERK decreased with treatment of Pal-pHK-pKV and pHK-pKV compared with the control group (*Figure 4A*), which indicates Pal-pHK-pKV and pHK-pKV inhibited the activation of the ERK signalling pathway. In line with the decreased ERK phosphorylation, the expression of BCL-2 decreased and the mRNA and protein expression levels of BAX increased after treatment with Pal-pHK-pKV and pHK-pKV (*Figure 4B,4C*). Meanwhile, Pal-pHK-pKV and pHK-pKV induced cytochrome c release from mitochondria to the cytoplasm (*Figure 4D*). Additionally, the relative expression of *FAS* increased with Pal-pHK-pKV and pHK-pKV treatment, as compared to the control group (*Figure 4E*).

Discussion

PTCL is heterogeneous disease comprising more than 20 subtypes with distinct biological characters and different prognoses. Compared with diffuse large B-cell lymphoma (DLBCL), PTCL patients have a worse prognosis with the traditional anthracycline-based treatment. Brentuximab vedotin, which is an anti-cluster of differentiation (CD) 30 antibody drug conjugate, has shown good efficacy as a second-line PTCL treatment (17). In the ECHELON-2 study, compared with CHOP, brentuximab vedotin plus

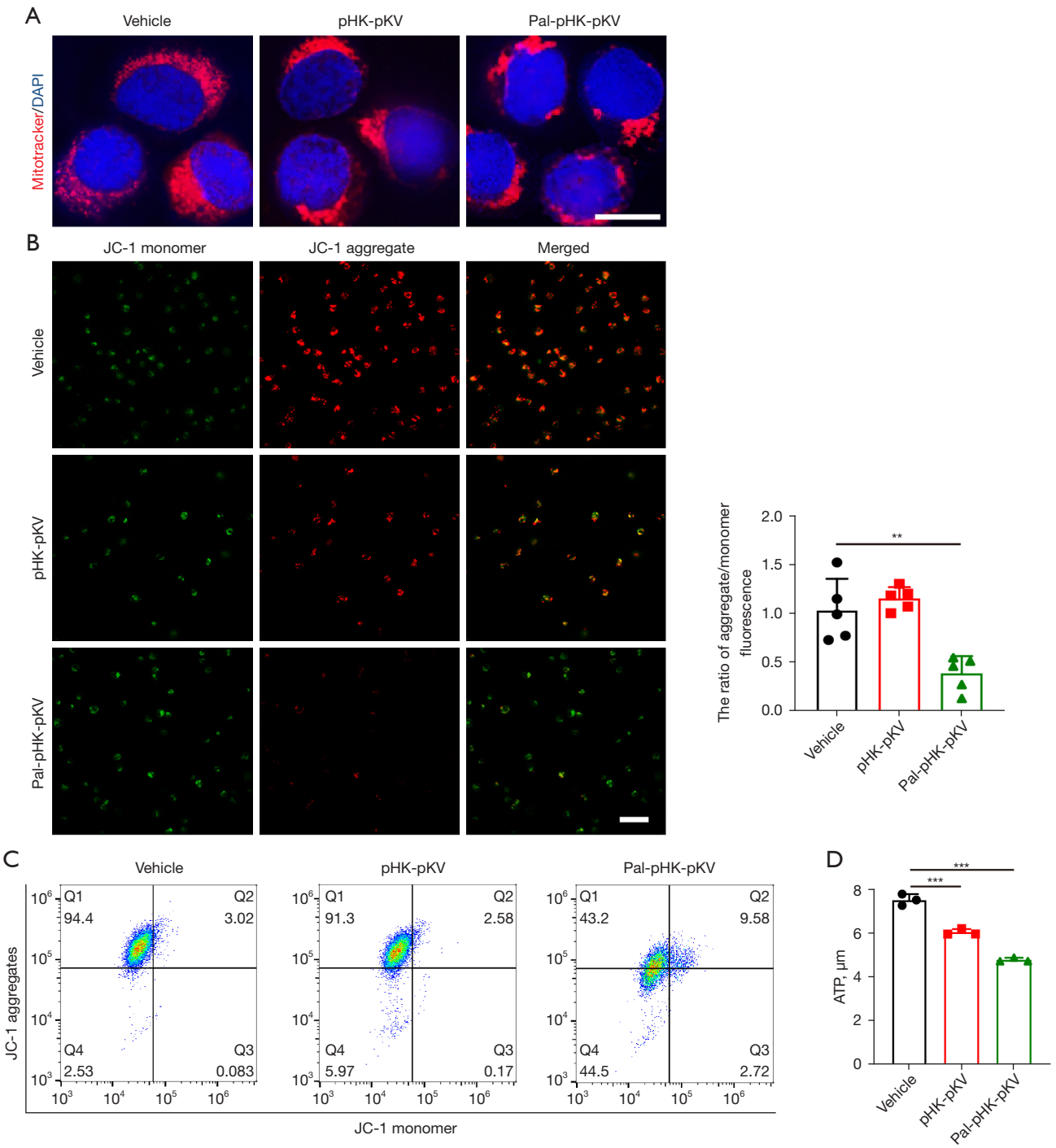

Figure 3 pHK-pKV and Pal-pHK-pKV induced mitochondrial dysfunction. (A) Representative confocal microscope images of the mitochondrial (red) in pHK-pKV or Pal-pHK-pKV-treated H9 cells. Scale bar =10 μm. (B) JC-1 staining of H9 cells treated with pHK-pKV and Pal-pHK-pKV. Red fluorescence represents the mitochondrial aggregate JC-1 and green fluorescence indicates the monomeric JC-1. Quantification ratio of aggregate/monomeric JC-1 (n=5 samples per group). (C) Flow cytometric analysis of JC-1-stained cells for the detection of mitochondrial membrane potential changes induced by pHK-pKV or Pal-pHK-pKV in H9 cells (n=3 samples per group). (D) Cellular ATP in H9 cells were measured after treatment with pHK-pKV and Pal-pHK-pKV (n=3 samples per group). **P<0.01; ***P<0.001. Data were presented as mean ± SD. JC-1 J-aggregates cyanine dye; ATP, adenosine triphosphate.

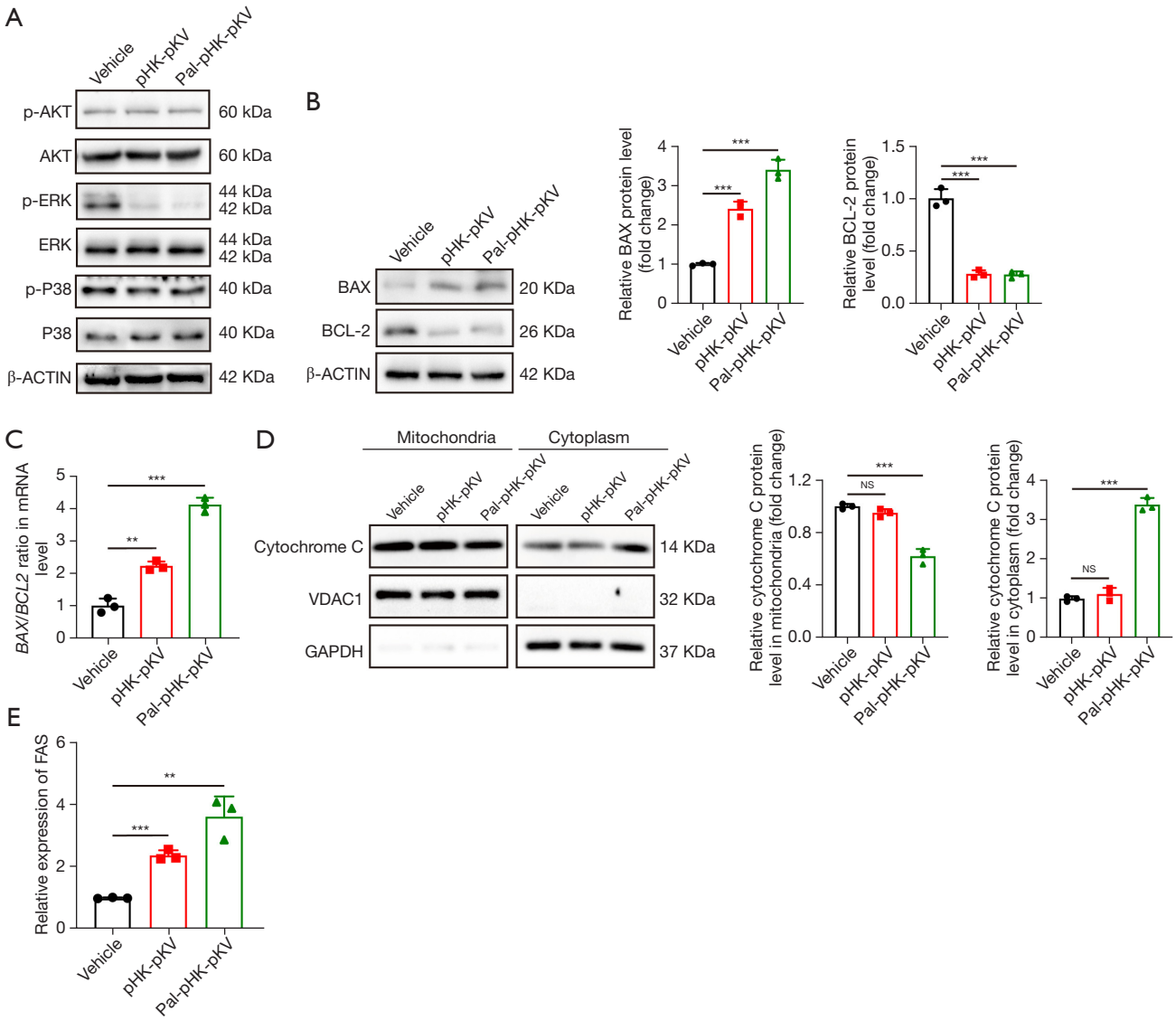

Figure 4 Mitochondria-specific peptide amphiphiles induced apoptosis via the ERK/BCL-2 pathway. (A) Phosphorylation of AKT, ERK, and P38 in H9 cells with pHK-pKV and Pal-pHK-pKV treatment. β-actin marks the loading level in each lane (n=3 samples per group). (B) Protein expression of BAX and BCL-2 in pHK-pKV and Pal-pHK-pKV-treated H9 cells. β-actin marks the loading level in each lane (n=3 samples per group). (C) The *BAX/BCL-2* mRNA ratio increased in H9 cells after pHK-pKV and Pal-pHK-pKV treatment (n=3 samples per group). (D) Cytochrome c expression of pHK-pKV and Pal-pHK-pKV-treated H9 cells in mitochondria and the cytoplasm was detected by western blot. VDAC1 and β-actin were included as a loading control (n=3 samples per group). (E) Transcriptional expression levels of *FAS* in H9 cells treated with pHK-pKV and Pal-pHK-pKV (n=3 samples per group). **P<0.01; ***P<0.001. Data were presented as mean ± SD. ERK, extracellular regulated protein kinases; BAX, cell lymphoma 2 associated X protein; BCL-2, B cell lymphoma 2; VDAC1, voltage-dependent anion channel 1.

cyclophosphamide, doxorubicin, prednisone (CHP) improved the 5-year OS rates from 61.0% in the CHOP group to 70.1% in the A + CHP group in frontline treatment (18). Although this is a promising outcome, only a small number of patients whose lymphoma cells expressed CD30 were included, and these CD30-positive patients have always shown a good prognosis. However, the outcomes of PTCL-NOS and AITL were disappointing,

partly due to the lack of effective therapeutic targets.

In recent years, gene expression profiling (GEP) and next-generation sequencing (NGS) have provided more information about the pathogeneses of PTCL, and shown that the TCR signalling pathway and epigenetic abnormality are present in most PTCL subtypes (19,20). Drugs targeting these abnormalities have been demonstrated to have a good clinical efficacy. For example, the histone deacetylase (HDAC) inhibitors (belinostat, romidepsin, and chidamide) have been approved for second-line treatment in PTCL (21-23). Considering that the PI3K-AKT pathway was active and negative regulators of the PI3K-AKT pathway were inactive in most PTCLs, the PI3K delta/gamma inhibitors, duvelisib and tenalisib, are in clinical development and have shown an objective response rate (ORR) of 45.7–50% in PTCL (24,25). However, at present, all of these target therapies can only provide a response rate of 20–50%. A good target, which is common in PTCL, may improve the response rate and prolong the survival of patients.

In recent years, researchers have found that mitochondria play a pivotal role in the occurrence and progression of cancer, and thus, mitochondria become a potential target in lymphoma treatments (26). It has been reported that HKII binds to VDAC1 at the mitochondrial outer membrane. Disrupting HKII-VDAC1 interaction and the VDAC1-based peptide can induce cell death in hepatocarcinoma cells and chronic lymphocytic leukemia cells (27-29). Pal-pHK-pKV and pHK-pKV are new mitochondria-specific peptide amphiphiles designed by Liu *et al.*, which can induce cell death in human lung cancer cells (16). In the present study, we demonstrated that Pal-pHK-pKV and pHK-pKV exerted anti-lymphoma activity in PTCL, and the inhibition ability of Pal-pHK-pKV was more pronounced than that of pHK-pKV, which was perhaps due to its enhanced cell penetrating capacity in the cancer cells. Moreover, Pal-pHK-pKV and pHK-pKV are safe for normal cells; treatment of the normal immortalized colon epithelial cell line (NCM460 cells) by Pal-pHK-pKV and pHK-pKV only caused a minor decrease in cell viability (16). Just like N-Terminal-Antp to normal hematologic cells, it exhibited only slightly effects on peripheral blood mononuclear cells (PBMCs) from healthy donors (29). So, Pal-pHK-pKV and pHK-pKV has a potential benefit in PTCL treatment, with safety.

VDAC1 is in the outer membrane of mitochondria, which allows for free shuttling of ATP from mitochondria to the cytosol and plays an important role in energy metabolism and energy balance (14). VDAC1 can also promote apoptosis mediated by mitochondria. A previous study showed that the metabolite exchange between the cytosol and mitochondria was decreased following the down-regulated expression of *VDAC1*, and as a result, cell growth was also inhibited (30). In the present study, we found that the production of ATP decreased with Pal-pHK-pKV and pHK-pKV treatment. The decrease of ATP in the cytosol then inhibited the downstream ERK signalling pathway, disrupted the BAX/BCL-2 balance in the outer membrane of the mitochondria, and induced cytochrome c release from mitochondria. Some studies have shown that ATP can activate the ERK signalling pathway (31), and ERK activation results in up-regulation of BCL-2 and cell survival (32). ATP can also promote cell survival via down-regulation of the BAX/BCL-2 ratio (33). Hence, decreased ATP in Pal-pHK-pKV and pHK-pKV-treated cells results in the release of cytochrome c via inhibition of the ERK pathway. In addition, it can also lead to an increased BAX/BCL-2 ratio and induce cell apoptosis. On the other hand, decreased ATP can induce apoptosis via an extrinsic pathway. A previous study showed that the FAS, FAS ligand, and FAS-associating protein with death domain (FADD) increased significantly in ATP-depleted canine kidney cells (34). Consistent with this, we found the *FAS* mRNA expression increased with Pal-pHK-pKV and pHK-pKV treatment. So, the mitochondria-specific peptides, Pal-pHK-pKV and pHK-pKV, targeted the interaction between VDAC1-HKII and inhibited the shuttle of ATP from mitochondria to the cytosol. The decreased ATP level in cytosol then inhibited the ERK/BCL-2 pathway and increased the BAX/BCL-2 ratio, resulting in the release of cytochrome c and the initiation of apoptosis through an intrinsic pathway. At the same time, Pal-pHK-pKV and pHK-pKV also initiated apoptosis through an extrinsic pathway by upregulating *FAS*. In summary, Pal-pHK-pKV and pHK-pKV inhibited the cell growth and exerted anti-tumor activity in PTCL (*Figure 5*).

In conclusion, mitochondria-specific peptides, Pal-pHK-pKV and pHK-pKV, provide a new approach in PTCL treatment. They have shown promising results and are expected to overcome drug resistance in PTCL. We speculate that Pal-pHK-pKV and pHK-pKV could combine with antineoplastic drugs as a new therapeutic approach for PTCL treatment. However, more research is needed to further explore their effects and safety in clinical practice.

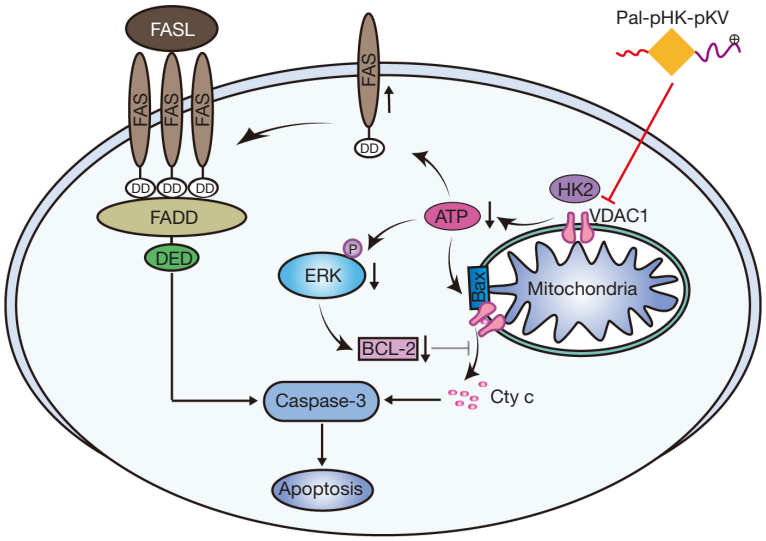

Figure 5 Mechanisms of mitochondria-specific peptides induction of PTCL apoptosis. Our work provides an example of the complex mechanisms of mitochondria-specific peptides amphiphiles induction of PTCL cell apoptosis and inhibition of tumor cell proliferation. In human PTCL cells, pHK-pKV and Pal-pHK-pKV block the interaction of VDAC1 and HKII, and detach HKII from mitochondria, which depolarizes the mitochondrial membrane potential, induces mitochondria dysfunction and decreases ATP production. The decreased ATP then inhibits activation of the ERK/BCL-2 pathway and increases the BAX/BCL-2 ratio then cytochrome c release from the mitochondria, and induces capase-3 activation and subsequently apoptosis. Additionally, decreased ATP can also induce the expression of FAS and subsequently apoptosis. PTCL, peripheral T-cell lymphomas; VDAC1, voltage-dependent anion channel 1; HKII, hexokinase II; ATP, adenosine triphosphate; ERK, extracellular regulated protein kinases; BCL-2, B cell lymphoma 2; BAX, BCL-2 associated X protein.

Acknowledgments

Funding: This work was supported by the National Natural Science Foundation of China (No. 81670177 to Q Zhang and No. 81970182 to J Zuo).

Footnote

Reporting Checklist: The authors have completed the MDAR reporting checklist. Available at https://atm.amegroups.com/article/view/10.21037/atm-22-2233/rc

Data Sharing Statement: Available at https://atm.amegroups.com/article/view/10.21037/atm-22-2233/dss

Conflicts of Interest: All authors have completed the ICMJE uniform disclosure form (available at https://atm.amegroups.com/article/view/10.21037/atm-22-2233/coif). The authors have no conflicts of interest to declare.

Ethical Statement: The authors are accountable for all aspects of the work in ensuring that questions related to the accuracy or integrity of any part of the work are appropriately investigated and resolved.

References

1. Rangoonwala HI, Cascella M. Peripheral T-Cell Lymphoma. Treasure Island (FL): StatPearls, 2022.
2. Savage KJ, Harris NL, Vose JM, et al. ALK-anaplastic large-cell lymphoma is clinically and immunophenotypically different from both ALK+ ALCL and peripheral T-cell lymphoma, not otherwise

specified: report from the International Peripheral T-Cell Lymphoma Project. Blood 2008;111:5496-504.
3. Savage KJ, Chhanabhai M, Gascoyne RD, et al. Characterization of peripheral T-cell lymphomas in a single North American institution by the WHO classification. Ann Oncol 2004;15:1467-75.
4. Armitage JO. The aggressive peripheral T-cell lymphomas: 2012 update on diagnosis, risk stratification, and management. Am J Hematol 2012;87:511-9.
5. Iqbal J, Weisenburger DD, Greiner TC, et al. Molecular signatures to improve diagnosis in peripheral T-cell lymphoma and prognostication in angioimmunoblastic T-cell lymphoma. Blood 2010;115:1026-36.
6. van der Weyden CA, Pileri SA, Feldman AL, et al. Understanding CD30 biology and therapeutic targeting: a historical perspective providing insight into future directions. Blood Cancer J 2017;7:e603.
7. Slupianek A, Nieborowska-Skorska M, Hoser G, et al. Role of phosphatidylinositol 3-kinase-Akt pathway in nucleophosmin/anaplastic lymphoma kinase-mediated lymphomagenesis. Cancer Res 2001;61:2194-9.
8. Dunn J, Grider MH. Physiology, Adenosine Triphosphate. Treasure Island (FL): StatPearls, 2022.
9. Almeida L, Lochner M, Berod L, et al. Metabolic pathways in T cell activation and lineage differentiation. Semin Immunol 2016;28:514-24.
10. Derynck R, Budi EH. Specificity, versatility, and control of TGF-β family signaling. Sci Signal 2019;12:eaav5183.
11. Lauterwasser J, Fimm-Todt F, Oelgeklaus A, et al. Hexokinases inhibit death receptor-dependent apoptosis on the mitochondria. Proc Natl Acad Sci U S A 2021;118:e2021175118.
12. Pastorino JG, Hoek JB. Regulation of hexokinase binding to VDAC. J Bioenerg Biomembr 2008;40:171-82.
13. Woldetsadik AD, Vogel MC, Rabeh WM, et al. Hexokinase II-derived cell-penetrating peptide targets mitochondria and triggers apoptosis in cancer cells. FASEB J 2017;31:2168-84.
14. Yang M, Sun J, Stowe DF, et al. Knockout of VDAC1 in H9c2 Cells Promotes Oxidative Stress-Induced Cell Apoptosis through Decreased Mitochondrial Hexokinase II Binding and Enhanced Glycolytic Stress. Cell Physiol Biochem 2020;54:853-74.
15. Bryan N, Raisch KP. Identification of a mitochondrial-binding site on the N-terminal end of hexokinase II. Biosci Rep 2015;35:00205.
16. Liu D, Angelova A, Liu J, et al. Self-assembly of mitochondria-specific peptide amphiphiles amplifying lung cancer cell death through targeting the VDAC1-hexokinase-II complex. J Mater Chem B 2019;7:4706-16.
17. Pro B, Advani R, Brice P, et al. Five-year results of brentuximab vedotin in patients with relapsed or refractory systemic anaplastic large cell lymphoma. Blood 2017;130:2709-17.
18. Horwitz S, O'Connor OA, Pro B, et al. The ECHELON-2 Trial: 5-year results of a randomized, phase III study of brentuximab vedotin with chemotherapy for CD30-positive peripheral T-cell lymphoma. Ann Oncol 2022;33:288-98.
19. Timmins MA, Wagner SD, Ahearne MJ. The new biology of PTCL-NOS and AITL: current status and future clinical impact. Br J Haematol 2020;189:54-66.
20. Heavican TB, Bouska A, Yu J, et al. Genetic drivers of oncogenic pathways in molecular subgroups of peripheral T-cell lymphoma. Blood 2019;133:1664-76.
21. Coiffier B, Pro B, Prince HM, et al. Results from a pivotal, open-label, phase II study of romidepsin in relapsed or refractory peripheral T-cell lymphoma after prior systemic therapy. J Clin Oncol 2012;30:631-6.
22. O'Connor OA, Horwitz S, Masszi T, et al. Belinostat in Patients With Relapsed or Refractory Peripheral T-Cell Lymphoma: Results of the Pivotal Phase II BELIEF (CLN-19) Study. J Clin Oncol 2015;33:2492-9.
23. Shi Y, Dong M, Hong X, et al. Results from a multicenter, open-label, pivotal phase II study of chidamide in relapsed or refractory peripheral T-cell lymphoma. Ann Oncol 2015;26:1766-71.
24. Horwitz SM, Koch R, Porcu P, et al. Activity of the PI3K-delta,gamma inhibitor duvelisib in a phase 1 trial and preclinical models of T-cell lymphoma. Blood 2018;131:888-98.
25. Huen A, Haverkos BM, Zain J, et al. Phase I/Ib Study of Tenalisib (RP6530), a Dual PI3K delta/gamma Inhibitor in Patients with Relapsed/Refractory T-Cell Lymphoma. Cancers (Basel) 2020;12:2293.
26. Kafkova A, Trnka J. Mitochondria-targeted compounds in the treatment of cancer. Neoplasma 2020;67:450-60.
27. Arbel N, Shoshan-Barmatz V. Voltage-dependent anion channel 1-based peptides interact with Bcl-2 to prevent antiapoptotic activity. J Biol Chem 2010;285:6053-62.
28. Prezma T, Shteinfer A, Admoni L, et al. VDAC1-based peptides: novel pro-apoptotic agents and potential therapeutics for B-cell chronic lymphocytic leukemia. Cell Death Dis 2013;4:e809.
29. Pittala S, Krelin Y, Shoshan-Barmatz V. Targeting Liver Cancer and Associated Pathologies in Mice with

a Mitochondrial VDAC1-Based Peptide. Neoplasia 2018;20:594-609.
30. Abu-Hamad S, Sivan S, Shoshan-Barmatz V. The expression level of the voltage-dependent anion channel controls life and death of the cell. Proc Natl Acad Sci U S A 2006;103:5787-92.
31. Huang L, Li B, Li W, et al. ATP-sensitive potassium channels control glioma cells proliferation by regulating ERK activity. Carcinogenesis 2009;30:737-44.
32. Wang C, Jin A, Huang W, et al. Up-regulation of Bcl-2 by CD147 Through ERK Activation Results in Abnormal Cell Survival in Human Endometriosis. J Clin Endocrinol Metab 2015;100:E955-63.
33. Song S, Jacobson KN, McDermott KM, et al. ATP promotes cell survival via regulation of cytosolic Ca2+ and Bcl-2/Bax ratio in lung cancer cells. Am J Physiol Cell Physiol 2016;310:C99-114.
34. Feldenberg LR, Thevananther S, del Rio M, et al. Partial ATP depletion induces Fas- and caspase-mediated apoptosis in MDCK cells. Am J Physiol 1999;276:F837-46.

(English Language Editor: A. Kassem)

Cite this article as: Sun Q, Gui A, Zou A, Yan Y, Qiu S, Zhu S, Liu W, Zuo J, Zhang Q, Yang L. Mitochondria-specific peptide amphiphiles induce mitochondrial dysfunction and peripheral T-cell lymphomas (PTCL) damage. Ann Transl Med 2022;10(10):570. doi: 10.21037/atm-22-2233

